Doctorate of Philosophy

Schrödinger's Catwalk

Brian Flynn

University of Bristol

December, 2020

CONTENTS

LIST OF TABLES

LIST OF FIGURES

LISTINGS

ACRONYMS

AIC	Akaike information criterion. 84, 86
AICC	Akaike information criterion corrected. 84
BF	Bayes factor. 25–27, 33, 35, 48, 51, 55, 57, 61, 63, 64, 80, 81, 87, 89–91, 93–95
BFEER	Bayes factor enhanced Elo ratings. 80, 81, 93, 94, 96
BIC	Bayesian information criterion. 86
CLE	classical likelihood estimation. 13
EDH	experiment design heuristic. 18–23, 26, 35, 45, 55, 56, 83
ES	exploration strategy. 27–31, 33–35, 40, 43, 45, 49, 51, 61, 65, 67, 75, 79, 105, 108
ET	exploration tree. 28, 29, 31, 33–35, 45, 47, 75
FH	Fermi-Hubbard. 58
FP	false negatives. 78
FP	false positives. 78
GA	genetic algorithm. iii, 34, 67, 71, 74, 75, 80, 82, 83, 88, 90, 93, 96–98
GES	genetic exploration strategy. 67, 78, 93, 94, 97
HPD	high particle density. 18
IQLE	interactive quantum likelihood estimation. 13, 14, 93, 94
LTL	log total likelihood. 16
ML	machine learning. 6, 26, 27, 78
MS	model search. 27–29, 31, 35, 43, 45
MVEE	minimum volume enclosing ellipsoid. 18

NV nitrogen-vacancy. 9
NVC nitrogen-vacancy centre. 14

OF objective function. iii, 67, 68, 74, 75, 78, 80, 81, 83, 84, 88, 91–93

PGH particle guess heuristic. 19, 20, 45

QHL quantum Hamiltonian learning. 8–14, 16, 18, 20–22, 25–27, 31–35, 40, 43, 48, 55, 56, 75, 93, 94, 105
QL quadratic loss. 17
QLE quantum likelihood estimation. 13, 32
QMLA Quantum Model Learning Agent. ii, iii, vii, 8, 13, 24, 25, 27–31, 34, 35, 40, 43–49, 51, 52, 60, 61, 63–65, 67, 72, 74–77, 83, 87, 88, 90, 91, 93, 94, 96–98, 105

SMC sequential monte carlo. 11–13, 15, 18, 19, 22, 31

TLTL total log total likelihood. 16, 25–27, 35, 84, 91
TN true negatives. 78
TP true positives. 78

GLOSSARY

Jordan Wigner transformation (JWT)	Jordan Wigner transformation . 60, 61, 64
Loschmidt echo (LE)	Quantum chaotic effect described. . 14
chromosome	A single candidate in the space of valid solutions to the posed problem in a genetic algorithm. . 68
gene	Individual element within a chromosome. . 68
hyperparameter	Variable within an algorithm that determines how the algorithm itself proceeds.. 11
instance	a single implementation of the QMLA algorithm. iii, 48, 94, 97, 98, 105
likelihood	Value that represents how likely a hypothesis is.. 10, 13, 15, 18, 31, 33, 34, 36, 88
model	The mathematical description of some quantum system. 24
model space	Abstract space containing all descriptions (within defined constraints such as dimension) of the system as models. 29
probe	Input probe state, $\|\psi\rangle$, which the target system is initialised to, before unitary evolution. plural. 13, 15, 18–22, 54
results directory	Directory to which the data and analysis for a given run of QMLA are stored. . 49
run	collection of QMLA instances. iii, vii, 48, 49, 64, 65, 94, 96, 98, 105
spawn	Process by which new models are generated by combining previously considered models.. 29
success rate	. 48, 49

term	Individual constituent of a model, e.g. a single operator within a sum of operators, which in total describe a Hamiltonian. . 24
volume	Volume of a parameter distribution's credible region.. 18, 55, 56, 63
win rate	. 48, 49

Part I

EXPERIMENTAL STUDIES

1

NITROGEN VACANCY CENTRE

It is of primary interest to apply the QMLA algorithm to real-life, experimental systems. In this chapter we devise an exploration strategy (ES) to operate in conjunction with experimental data in order to characterise an electron spin in an NV centre in diamond. In particular, we model, through Hamiltonian terms, interactions between the spin and the spin bath in which it resides, so that QMLA is finding an effective model for the open system dynamics.

1.1 NV-centres

NV centers are point defects in diamond, occuring naturally or synthetically. A nitrogen-14 (^{14}N) isotope is embedded in a lattice of carbon atoms in diamond, specifically such that the ^{14}N is in a cluster with three carbon-13 (^{13}C) isotopes as well as a lattice vacancy. Of the ^{14}N atom's five valence electrons, three bond with nearby ^{13}Cs; the remaining two unbonded electrons form a *lone pair* in the lattice. Such systems consisting of two spin-$\frac{1}{2}$ particles have been thoroughly studied; of particular interest are the resultant triplet states, i.e. the allowed permutations of the two electrons with total quantum spin $S = 1$, with magnetic spin multiplicity allowing $m_s = -1, 0, 1$, giving rise to distinct energy levels for the system. In the absence of a magnetic field, the states corresponding to $|m_s = \pm 1\rangle$ are degenerate, but in the presence of a magnetic field, B, they have distinct energy levels, referred to as hyperfine splitting.

A *manifold* is a set of states differing only slightly, for example states near the absolute ground state manifold might differ only in magnetic spin quantum number, and can be characterised as the ground state manifold. We consider two principle manifolds of the system: the ground state and excited manifolds, each consisting of three states, corresponding to the magnetic spin m_s. For brevity, we denote states with reference to their magnetic spin and manifold, e.g. the state in the ground state manifold with $m_s = 0$ is denoted $|m_s = 0\rangle_g$.

We designate the state $|m_s = 0\rangle_g$ as the basis state $|0\rangle = \begin{pmatrix} 1 \\ 0 \end{pmatrix}$, and $|m_s = -1\rangle_g$ as $|1\rangle = \begin{pmatrix} 0 \\ 1 \end{pmatrix}$, such that we have defined a qubit and computational basis. By shining a laser of 637nm (green) on the NVC, it is excited to the excited manifold, from which it decays back to the ground state manifold. Importantly, the process of this decay can be exploited for the preparation of the NVC in the computational basis state $|0\rangle$. That is, the dominant decay process from $|m_s = 0\rangle_e$ is spin-preserving, so it ends in $|m_s = 0\rangle_g$. On the other hand, had the NVC been in the $|m_s = \pm 1\rangle_e$, the dominant decay process is through a shelving (singlet) state, and does not preserve spin, such that it also decays to the $|m_s = 0\rangle_g$. Therefore, irrespective of the initial state, by shining the green laser on the NVC, it is most likely that it has been prepared in $|m_s = 0\rangle_g = |0\rangle$, providing us a starting point from which to perform computation.

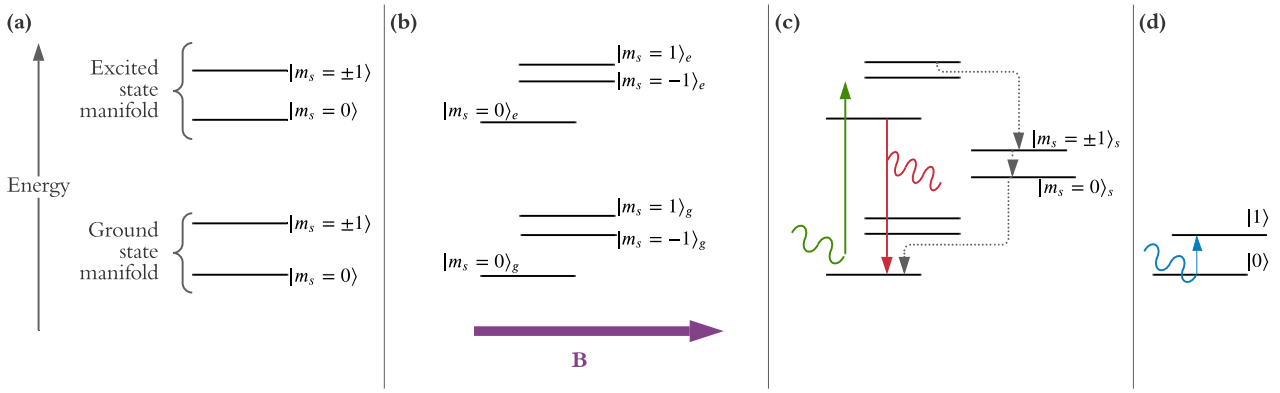

Figure 1.1: nitrogen-vacancy centre energy levels. **a**, With no external field, the system simply has excited and ground-state manifolds, each of which consist of two energy levels depending on the magnetic spin, m_s. **b**, In the presence of a magnetic field (purple, B), the magnetic spins have distinct energy levels, i.e. hyperfine splitting. States are denoted by their magnetic spin and subscripted by their manifold. **c**, Application of a green ($637nm$) laser excites the nitrogen-vacancy centre (NVC) from any of the states in the ground state manifold to the excited manifold. The dominant decay mechanism for the excited states are shown: (i) $|m_s = 0\rangle_e \rightarrow |m_s = 0\rangle_g$ (red line) through the emission of a red photon; (ii) $|m_s = \pm 1\rangle_e \rightarrow |m_s = 0\rangle_g$ (dotted grey lines) via the shelving manifold which allows for non-spin-preserving transition, and does not emit a photon. **d**, Computational basis states $|0\rangle$ and $|1\rangle$ are assigned to the two lowest energy states. The difference in energy between these states is such that a microwave (MW, blue) photon can trigger transition from $|0\rangle$ to $|1\rangle$.

We can further exploit the decay mechanism to compose a readout procedure, to infer the population of $\{|0\rangle, |1\rangle\}$ at a given instant, for example following the application of gates to the system. We know that the excitation due to the green laser is spin-preserving, i.e. when the NVC is in $|m_s = 0\rangle_e$, it had originated in $|m_s = 0\rangle_g$. We also know that the decay $|m_s = 0\rangle_e \to |m_s = 0\rangle_g$ is spin preserving, with the emission of a red photon: by simply counting the number of photons emitted, we quantify the population of $|0\rangle$ at the time of query. On the contrary, when the $|m_s = -1\rangle_g$ is excited, spin is also preserved, so it goes to $|m_s = -1\rangle_e$; but $|m_s = -1\rangle_e$ decays through the shelving state as outlined earlier, *without* the emission of a photon. We can hence infer the population of $|m_s = -1\rangle_g$ at the time of query by the fraction of incidents which don't emit a photon.

In summary then, by assigning basis states $|0\rangle, |1\rangle$ to energy levels of the ground state manifold, we are able to ensure the preparation of the NVC in $|0\rangle$ by first shining a green laser on the NVC. We can then apply microwave radiation to achieve quantum logical gates on the system, and read out the final state of the system, again by shining a green laser and observing the emitted photons (photoluminescence (PL)) and inferring the population level of each basis state. We represent these concepts in a simplified format in Section 1.1.

1.2 TARGET SYSTEM

Assuming the magnetic field aligns with the z-axis of the spin, the total interactions the spin is subject to are:

- ground state energy splitting, Δ_{gs}

1.2.1 *Short time dynamics*

1.3 EXPLORATION STRATEGY

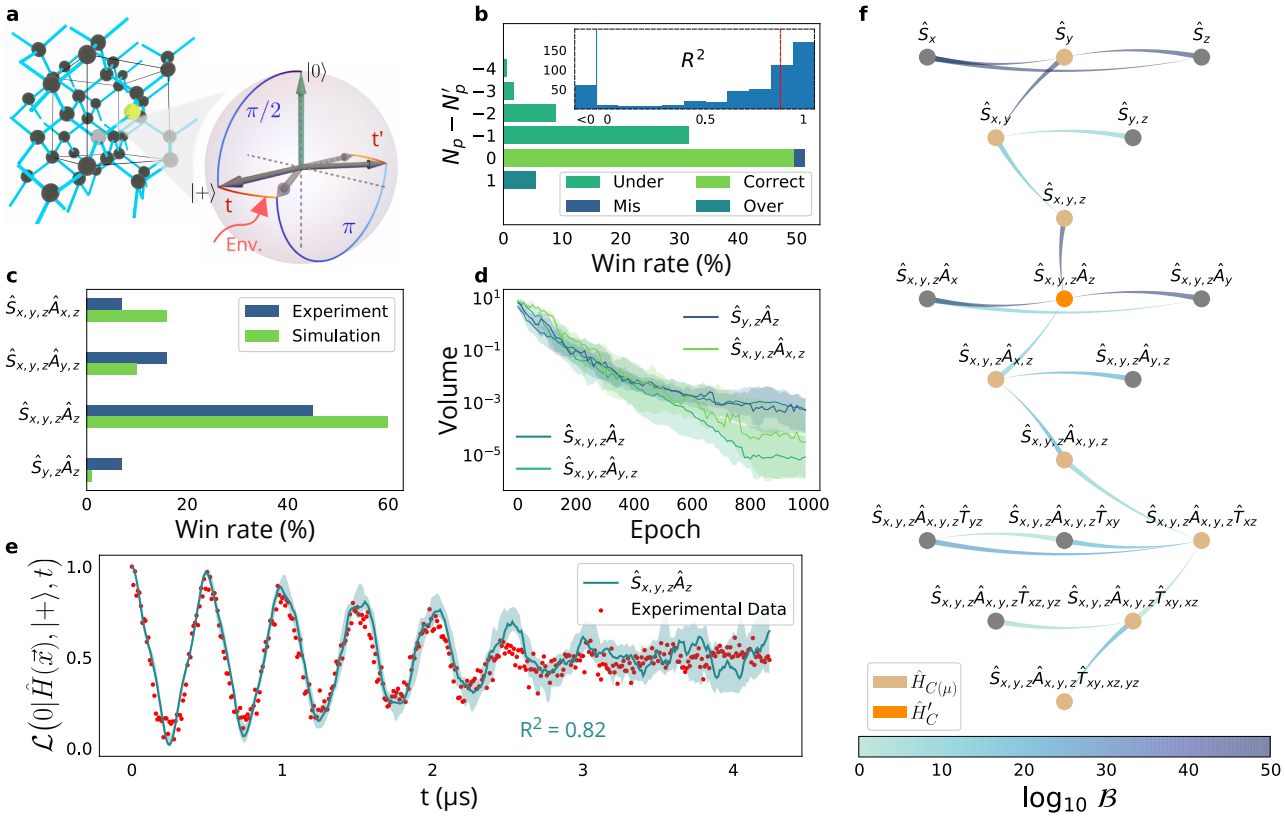

Figure 1.2: **a**, The carbon lattice providing the outer environment for the NV centre, along with the time evolution of the electron spin state (represented on a Bloch sphere) during the pulses for the Hahn-echo sequences. The final $\pi/2$ pulse is omitted. **b**, Simulation of 500 independent QMLA instances, where $\hat{H}_0$ is chosen randomly. The win rate is reported against the difference $(N_p - N'_p)$ between the number of parameters in the QMLA-selected ($\hat{H}'$) and true models, respectively. The *under-parameterised* *(over-parameterised)* class refers to models with less (more) parameters than $\hat{H}_0$. *Correct* indicates that exactly $\hat{H}_0$ was found. The *mis-parameterised* class groups models with the same parametrisation cardinality as $\hat{H}_0$, but different Hamiltonian terms. **Inset**, Histogram of occurrences of R^2 values for each retrieved $\hat{H}'$ against a sampling of datapoints from $\hat{H}_0$, with median $R^2 = 0.84$ (red dotted line). **c**, Win rates of top four models (see main text), for 100 QMLA instances, against both simulated and experimental data. Simulations use $\hat{H}_0 =$. **d**, Total volume spanned by the parameters' prior across epochs, for the models in **c**. Shaded areas indicate 66% credible regions. **e**, Simulated likelihoods reproduced by the model with the highest win rate ($\hat{S}_{x,y,z}\hat{A}_z$, turquoise), compared with corresponding NV-centre system experimental data (red-dots, extracted from the observed PL of the first microseconds in Hahn-echo decay). Error bars smaller than the dots (see Methods). **f**, A single QMLA instance against experimental data in **e**, depicted as a , see Fig. **??**c. The thin end of each edge points to the favoured model; the colour of the edges maps $\log_{10}\mathcal{B}$ as in the bar legend at the bottom. Layer champions are in light brown, whereas the global champion $\hat{H}'$ is in orange.

2

EXTENSION TO MANY QUBITS

2.1 GENETIC ALGORITHM

APPENDIX

A

FIGURE REPRODUCTION

Most of the figures presented in the main text are generated directly by the QMLA framework. Here we list the implementation details of each figure so they may be reproduced by ensuring the configuration in Table A.1 are set in the launch script. The default behaviour of QMLA is to generate a results folder uniquely identified by the date and time the run was launched, e.g. results can be found at the *results directory* qmla/Launch/Jan_01/12_34. Given the large number of plots available, ranging from high-level run perspective down to the training of individual models, we introduce a plot_level $\in \{1, ..., 6\}$ for each run of QMLA: higher plot_level informs QMLA to generate more plots.

Within the results directory, the outcome of the run's instances are stored, with analysis plots broadly grouped as

- evaluation: plots of probes and times used as the evaluation dataset.
- single_instance_plots: outcomes of an individual QMLA instance, grouped by the instance ID. Includes results of training of individual models (in model_training), as well as sub-directories for anlaysis at the branch level (in branches) and comparisons.
- combined_datasets: pandas dataframes containing most of the data used during analysis of the run. Note that data on the individual model/instance level may be discarded so some minor analyses can not be performed offline.
- exploration_strategy_plots plots specifically required by the ES at the run level.
- champion_models: analysis of the models deemed champions by at least one instance in the run, e.g. average parameter estimation for a model which wins multiple instances.
- performance: evaluation of the QMLA run, e.g. the win rate of each model and the number of times each term is found in champion models.
- meta analysis of the algorithm' implementation, e.g. timing of jobs on each process in a cluster; generally users need not be concerned with these.

In order to produce the results presented in this thesis, the configurations listed in Table A.1 were input to the launch script. The launch scripts in the QMLA codebase consist of many configuration settings for running QMLA; only the lines in snippet in Listing A.1 need to be set according to altered to retrieve the corresponding figures. Note that the runtime of QMLA grows quite quickly with N_E, N_P (except for the AnalyticalLikelihood ES), especially for the entire QMLA algorithm; running quantum Hamiltonian learning (QHL) is feasible on a personal computer in < 30 minutes for $N_e = 1000; N_p = 3000$.

```
#!/bin/bash
```

```
###############
# QMLA run configuration
###############
num_instances=1
run_qhl=1 # perform QHL on known (true) model
run_qhl_mulit_model=0 # perform QHL for defined list of models.
exp=200 # number of experiments
prt=1000 # number of particles

###############
# QMLA settings
###############
plot_level=6
debug_mode=0

###############
# Choose an exploration strategy
###############

exploration_strategy='AnalyticalLikelihood'
```

Listing A.1: "QMLA Launch scipt"

Figure	Exploration Strategy	Algorithm	N_E	N_P	Data
??	AnalyticalLikelihood	QHL	500	2000	Nov_16/14_28
??	DemoIsing	QHL	500	5000	Nov_18/13_56
??	DemoIsing	QHL	1000	5000	Nov_18/13_56
??	DemoIsing	QHL	1000	5000	Nov_18/13_56
??	IsingLatticeSet	QMLA	1000	4000	Nov_19/12_04
	IsingLatticeSet	QMLA	1000	4000	Sep_30/22_40
??	HeisenbergLatticeSet	QMLA	1000	4000	Oct_22/20_45
	FermiHubbardLatticeSet	QMLA	1000	4000	Oct_02/00_09
	DemoBayesFactorsByFscore	QMLA	500	2500	Dec_09/12_29
??	DemoFractionalResourcesBayesFactorsByFscore	QMLA	500	2500	Dec_09/12_29
	DemoBayesFactorsByFscore	QMLA	1000	5000	Dec_09/12_29
	DemoBayesFactorsByFscoreEloGraphs	QMLA	500	2500	Dec_09/12_29

Table A.1: Implementation details for figures used in the main text.

B

EXAMPLE EXPLORATION STRATEGY RUN

A complete example of how to run the ;sqmla framework, including how to implement a custom ES, and generate/interpret analysis, is given.

BIBLIOGRAPHY